

# Synthesis, Magnetic Anisotropy and Optical Properties of Preferred Oriented Zinc Ferrite Nanowire Arrays

Daqiang Gao · Zhenhua Shi · Yan Xu · Jing Zhang ·  
Guijin Yang · Jinlin Zhang · Xinhua Wang ·  
Desheng Xue

Received: 10 April 2010 / Accepted: 6 May 2010 / Published online: 22 May 2010  
© The Author(s) 2010. This article is published with open access at Springerlink.com

**Abstract** Preferred oriented  $\text{ZnFe}_2\text{O}_4$  nanowire arrays with an average diameter of 16 nm were fabricated by post-annealing of  $\text{ZnFe}_2$  nanowires within anodic aluminum oxide templates in atmosphere. Selected area electron diffraction and X-ray diffraction exhibit that the nanowires are in cubic spinel-type structure with a [110] preferred crystallite orientation. Magnetic measurement indicates that the as-prepared  $\text{ZnFe}_2\text{O}_4$  nanowire arrays reveal uniaxial magnetic anisotropy, and the easy magnetization direction is parallel to the axis of nanowire. The optical properties show the  $\text{ZnFe}_2\text{O}_4$  nanowire arrays give out 370–520 nm blue-violet light, and their UV absorption edge is around 700 nm. The estimated values of direct and indirect band gaps for the nanowires are 2.23 and 1.73 eV, respectively.

**Keywords**  $\text{ZnFe}_2\text{O}_4$  · Nanowire arrays · Preferred oriented · Magnetic anisotropy · Optical properties

## Introduction

As an important member of ferrite family, nanometer-sized spinel  $\text{ZnFe}_2\text{O}_4$  has received growing interest from the

fundamental and experimental point of view because of its potential application in gas sensors with high sensitivity and low-energy consumption [1–4]. Besides, the nanometer-sized  $\text{ZnFe}_2\text{O}_4$  is considered as a promising semiconductor photocatalyst for various photochemical processes, such as photoelectric conversion and photochemical hydrogen production from water, owing to its ability to absorb visible light, high efficiency, low cost, and excellently photochemical stability [5–7]. Meanwhile, the nanometer-sized  $\text{ZnFe}_2\text{O}_4$  shows unusual magnetic properties compared to the bulk form [8], such as high Curie temperature and large magnetization at room temperature (RT) have been observed in  $\text{ZnFe}_2\text{O}_4$  nanoparticles and films [9–12]. The issue has been extensively researched and ascribed to the dominant role of oxygen vacancies [13], surface effects [14], as well as cation random distribution of magnetic  $\text{Fe}^{3+}$  ions and diamagnetic  $\text{Zn}^{2+}$  ions among the interstitial octahedral (*B*) and tetrahedral (*A*) sites [15].

One-dimensional nanostructures can provide versatile building blocks for fabricating functional nanoscale electronic, optoelectronic, biomedical devices, magnetic and optical properties based on the bottom-up paradigm [16–20]. Recently, arrays of Ru, Pt, and PtRu nanowires and nanotubes were prepared by electrodeposition through the porous structure of an anodic aluminum oxide (AAO) membrane [21]. Iron-based 1D nanostructures have been successfully prepared using an electrospinning technique and varying the pyrolysis atmospheres [22]. Besides, 1D magnetic  $\text{MFe}_2\text{O}_4$  ( $\text{M} = \text{Co}, \text{Ni}$  and  $\text{Mn}$ ) nanomaterials also have been fabricated owing to their unique application in mesoscopic physics and nanoscale devices excellent properties [23–25]. For zinc ferrite, Liu et al. fabricated  $\text{ZnFe}_2\text{O}_4$  nanowires exhibiting unusual magnetic behavior by the thermal decomposition of the precursors inside silica

D. Gao · Z. Shi · J. Zhang · G. Yang · J. Zhang · X. Wang ·  
D. Xue (✉)

Key Lab for Magnetism and Magnetic Materials of the Ministry of Education, Lanzhou University, 730000 Lanzhou, People's Republic of China  
e-mail: xueds@lzu.edu.cn

Y. Xu  
Department of Physics, Xinxiang University, 453003 Xinxiang, People's Republic of China

host SBA-15 template [26]. By using a facile sol–gel AAO template method, Zhang and Liu et al. got highly ordered  $\text{ZnFe}_2\text{O}_4$  nanotube arrays, which displayed low-energy consumption and high sensitivity to organics as gas sensor materials and exhibited unusual photovoltaic behavior [7, 27]. However, all these 1D  $\text{ZnFe}_2\text{O}_4$  nanostructures have no orientation, where Kim et al. demonstrated that ordered ZnO microrod arrays with the preferred orientation of [0001] direction showing a strong free-exciton emission at 3.23 eV and a weak deep level emission at 2.2 eV reveals the high optical quality than that of the ZnO nanowire arrays with no orientation [28, 29].

Recently, Zhang and Zhu et al. demonstrated that the properties of 1D nanostructures depend strongly not only on the ordered arrangement but also on the crystal orientation as well [30, 31]. In our previous, the ordered  $\text{CoFe}_2\text{O}_4$  nanowire arrays with preferred crystal orientation were prepared by using the template synthesis in conjunction with electrochemical deposition [32]. Here, ordered  $\text{ZnFe}_2\text{O}_4$  nanowire arrays with preferred crystal orientation of [110] direction were prepared by spatial confinement oxidation of preferred [110] crystal orientation  $\text{ZnFe}_2$  alloy nanowires in AAO templates. The magnetic and optical properties of  $\text{ZnFe}_2\text{O}_4$  nanowire arrays were studied.

## Experiment

AAO was used as the template to synthesize  $\text{ZnFe}_2\text{O}_4$  nanowire arrays. The AAO templates were prepared through two anodizing steps as our report previously [33]. Briefly, high purity (99.999%) aluminum foil was polished in the mixed solution of ethanol and chloric acid ( $\text{HClO}_4$ ) in the constant current of 1.5 A for 5 min. The two-step anodization process was carried out in constant voltage mode to improve the arrangement of the ordered nanopore arrays. In the first step of the anodization, aluminum foil was anodized in 0.3 M  $\text{H}_2\text{SO}_4$  aqueous solution under the constant voltage of 13 V at 0°C for 0.5 h resulting in the textured surface, and then the formed anodic alumina layer was removed in the mixed solution of 0.4 M phosphoric acid and 0.2 M chromic acid at 60°C. Subsequently, the foil was re-anodized for 4 h using the same parameters in the first step. The electrolyte contained  $\text{FeSO}_4 \cdot 7\text{H}_2\text{O}$  (22 g/l),  $\text{ZnSO}_4 \cdot 7\text{H}_2\text{O}$  (10 g/l),  $\text{H}_3\text{BO}_3$  (10 g/l) with the *pH* value of 3.2. The alternating current electrodeposition was conducted at 200 Hz and 13 V for the duration of 5 min. The compositions in the ZnFe alloy nanowires were analyzed by energy dispersive X-ray spectroscopy (EDS) and inductively coupled plasma-atomic emission spectrometer (IRIS, ER/S). The results indicate the atom ratio of Fe:Zn is about 2. Because of the confinement of the nanopore size,

after heat treating the well orientation  $\text{ZnFe}_2$  alloy nanowire arrays in tube furnace at 460°C for 21 h in atmosphere, the arrays of  $\text{ZnFe}_2\text{O}_4$  nanowires inside the AAO templates with preferred crystallite orientation were obtained.

The morphologies of the nanowires were obtained by using the scanning electron microscope (SEM, Hitachi S-4800) and transmission electron microscopy (TEM, JEM-2010), where the nanowires were separated from the AAO templates by dissolving the aluminium oxide templates in the mixed solution of 0.2 M  $\text{H}_2\text{CrO}_4$  and 0.4 M  $\text{H}_3\text{PO}_4$ . The selected area electron diffraction (SAED) and X-ray diffraction (XRD, X' Pert PRO PHILIPS with Cu K $\alpha$  radiation) were employed to study the structure of the nanowires. The measurements of magnetic properties were made using Quantum Design MPMS magnetometer based on superconducting quantum interference device (SQUID) and vibrating sample magnetometer (VSM, Lakeshore 7304). Micro photoluminescence (PL) measurement was carried out at room temperature (RT) using a He-Cd laser with the wavelength of 325 nm and output power of 15 W as the excitation source. Light absorption property was measured using a UV–vis spectrophotometer (JASCO, UV-550).

## Results and Discussion

Figure 1a shows the cross-sectional SEM image of  $\text{ZnFe}_2\text{O}_4$  nanowires within AAO template. It is found that the nanowire arrays are ordered in AAO templates, and the average diameter is about 16 nm with the aspect ratio of 125. The EDS spectrum of the sample is shown in the inset of Fig. 1a, which reveals that the atom ratio of Zn: Fe is 32.3:67.7 (about 1:2), the same as the result of ICP. Shown in Fig. 1b is the TEM image of  $\text{ZnFe}_2\text{O}_4$  nanowires, which has a diameter consistent with the result of SEM. Figure 1c shows the high resolution TEM image of the corresponding  $\text{ZnFe}_2\text{O}_4$  nanowires. The lattice fringe between the two adjacent planes is about 0.30 nm apart, which is equal to the lattice fringes of the standard  $\text{ZnFe}_2\text{O}_4$ , growing along the [220] direction. The SAED pattern taken from the nanowires is shown in Fig. 1d, consisting of five obvious rings, which are corresponding to (220), (311), (400), (511), and (440) planes of polycrystalline  $\text{ZnFe}_2\text{O}_4$  with a cubic spinel-type lattice structure [34].

XRD patterns of the  $\text{ZnFe}_2$  and  $\text{ZnFe}_2\text{O}_4$  nanowire arrays within AAO templates are shown in Fig. 2a, b, respectively. Besides the smooth amorphous broad peak which comes from the AAO template, there is a sharp peak in XRD pattern of  $\text{ZnFe}_2$  nanowire arrays implying that orientation of [110] is perfect preferred. Similarly, the diffraction peaks of  $\text{ZnFe}_2\text{O}_4$  nanowire arrays shown in

**Fig. 1** **a** planar view SEM image of  $\text{ZnFe}_2\text{O}_4$  nanowires within AAO templates and corresponding EDS result is shown in the inset **b** TEM image **c** HRTEM image and **d** SAED pattern of  $\text{ZnFe}_2\text{O}_4$  nanowires

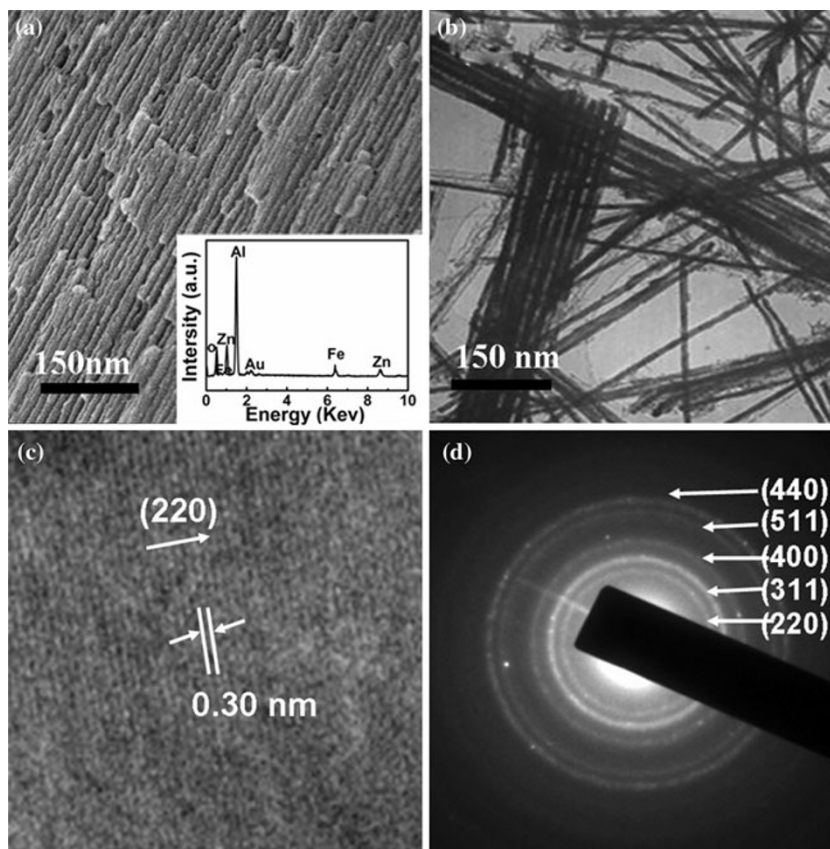


Fig. 2b can be indexed as (220), (311), and (440) of spinel-type lattice structure, and the [220] texture is along the axis of the  $\text{ZnFe}_2\text{O}_4$  nanowire arrays. XRD pattern of the  $\text{ZnFe}_2\text{O}_4$  powders is shown in the inset of Fig. 1b for comparison.

The schematic of the possible formation process of preferred oriented  $\text{ZnFe}_2\text{O}_4$  nanowire arrays is shown in Fig. 2c. The process could be described as:  $\text{ZnFe}_2 + 2\text{O}_2 \rightarrow \text{ZnFe}_2\text{O}_4$ . The XRD result shows that the  $\text{ZnFe}_2$  alloy nanowires have the preferred [110] crystal orientation along the axis of nanowires, which combined with the minor holes of AAO templates playing an important role to make the growth of  $\text{ZnFe}_2\text{O}_4$  nanowire arrays largely guide along the nanowire axis direction when heat treated. To sum up, there are two main conditions that make the nanowire arrays prefer crystal orientation: the one is the well orientation of original metal crystal, and the other is the spatial confinement of the minor hole.

The magnetic hysteresis loops recorded at 300 and 80 K using SQUID for  $\text{ZnFe}_2\text{O}_4$  nanowire arrays within AAO templates are shown in Fig. 3, where // and  $\perp$  represent that the applied field  $H$  is parallel and perpendicular to the major nanowire axis, respectively. The slope of the linear contribution in the saturation region has been subtracted. It

can be seen that the magnetic hysteresis loops in parallel and perpendicular directions at both 300 and 80 K are separating, indicating the existence of magnetic anisotropy for preferred oriented  $\text{ZnFe}_2\text{O}_4$  nanowire arrays, and magnetic easy axis is directed along the wire axis. Nearly, zero coercive forces are observed at 300 K both in the parallel and in the perpendicular direction ( $H_{c//} = 5$  Oe and  $H_{c\perp} = 3$  Oe). The magnetic hysteresis loops measured at 80 K indicate the coercivity ( $H_c$ ) and squareness ratio ( $M/M_s$ ) are about 290 Oe ( $H_{c//}$ ), 125 Oe ( $H_{c\perp}$ ), 0.21 ( $M/M_{s//}$ ), and 0.08 ( $M/M_{s\perp}$ ), respectively, where the magnified view of the magnetic hysteresis loops is shown in right bottom insets in Fig. 3a and b, respectively. The magnetic hysteresis loops of  $\text{ZnFe}_2$  nanowire arrays within AAO templates recorded at RT by VSM are shown in left top inset of Fig. 3a for compared.

As we known, bulk Zn-ferrite belongs to the normal spinel structure with paramagnetic properties at RT and long range antiferromagnetic order below 10 K [35]. However, nanocrystalline zinc ferrite is of great interest due to its unique magnetic properties that differ substantially from its bulk counterpart [10]. The occupancy of  $\text{Fe}^{3+}$  ions on both A- and B-sites leads to strong negative superexchange interaction between  $\text{Fe}^{3+}$  ions with large

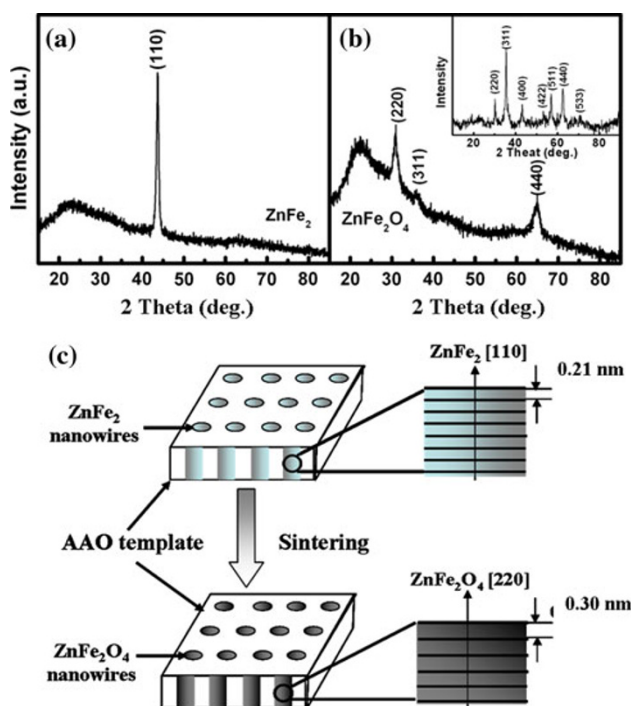


**Fig. 2** **a** XRD patterns of  $\text{ZnFe}_2$  and **b**  $\text{ZnFe}_2\text{O}_4$  nanowire arrays within AAO templates. The inset in Fig. 2b is the XRD pattern of  $\text{ZnFe}_2\text{O}_4$  powders for comparison. **c** Schematic illustration of the crystal growth process for  $\text{ZnFe}_2\text{O}_4$  nanowire arrays

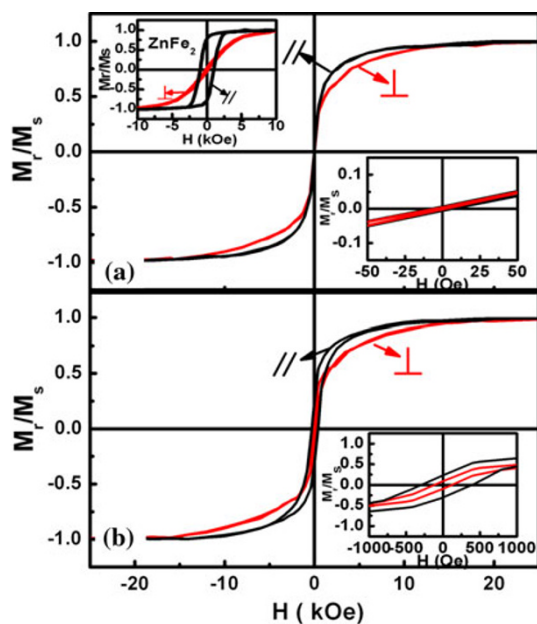


**Fig. 3** Magnetic hysteresis loops of the  $\text{ZnFe}_2\text{O}_4$  nanowires within AAO measured with the applied field parallel and perpendicular to the axis of the nanowires at **(a)** 300 K and **(b)** 80 K by SQUID. The magnified view of the magnetic hysteresis loops is shown in *right bottom insets* of Fig. 3a and b, respectively. RT magnetic hysteresis loops of  $\text{ZnFe}_2$  nanowire arrays within AAO templates measured using VSM are shown in *left top inset* of Fig. 3a

magnetization values. In our experiment, when  $\text{ZnFe}_2$  alloy nanowires were post-oxidation annealed, defects and the disorder of cation redistribution on *A*- and *B*- sites may occur, which can induce the magnetization for  $\text{ZnFe}_2\text{O}_4$  nanowire arrays in our case.

For the spinel ferrite, the easy axis of magnetization is  $[100]$ , and the hard one is  $[111]$ . The axis  $[110]$  is between them having the angle ( $\theta$ ) of  $45^\circ$  with the  $[100]$  and  $[111]$  directions, respectively. The total anisotropy is determined by the magnetostatic energy and the magnetocrystalline anisotropy energy. As the nanowires are oriented in polycrystals with high aspect ratio of 125, the easy magnetization direction determined by magnetostatic energy is along the axis of the nanowires. It can be seen from Fig. 4, the angle of  $\alpha$  is not fixed but changed from  $0^\circ$  to  $360^\circ$  in *xy* plane. So we presumed that the distribution of  $[100]$  may be like a conical axis shown in Fig. 4. When the applied field  $H$  is parallel to the nanowire axis ( $[110]$  direction), the magnetic moment components in *xy* plane cancel out each other, while the magnetic moment components in  $[110]$  direction are summed up. Owing to the high aspect ratio of the nanowires, it is concluded from earlier analyses that the easy magnetization axis of the nanowires is along the axis direction.

We further perform the PL spectroscopy to explore the optical properties of the  $\text{ZnFe}_2\text{O}_4$  nanowires. Figure 5 illustrates the RT PL spectra of  $\text{ZnFe}_2\text{O}_4$  nanowire arrays within AAO templates. The broadband visible emission band is observed in the entire PL spectrum, which can be fitted by two main emission bands: one is in the blue light region, and the other is in the violet light one. The blue emission around 468 nm can be assigned to intrinsic defects, particularly interstitial zinc defects [36]. And the same violet emission around 412 nm was also observed in excessive 50% Fe doped ZnO nanostructure where this luminescence was considered to be significantly contributed by the  $\text{ZnFe}_2\text{O}_4$  phase [37], which is corresponding to

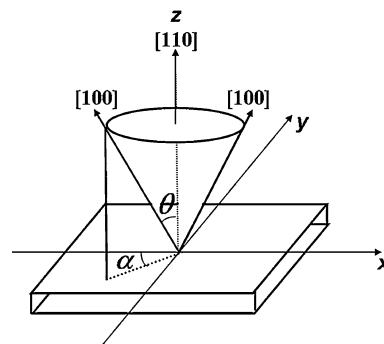


**Fig. 4** Schematic illustration of easy magnetization axis and distribution of  $[100]$  direction for preferred oriented  $\text{ZnFe}_2\text{O}_4$  nanowire arrays

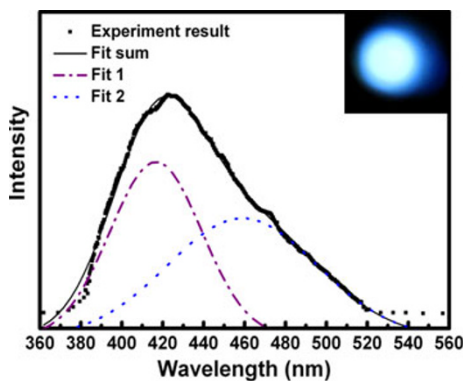


**Fig. 5** PL spectra of ZnFe<sub>2</sub>O<sub>4</sub> nanowire arrays within AAO templates measured at RT, and the image captured by camera indicates that the sample gives out blue-violet light is shown in the inset

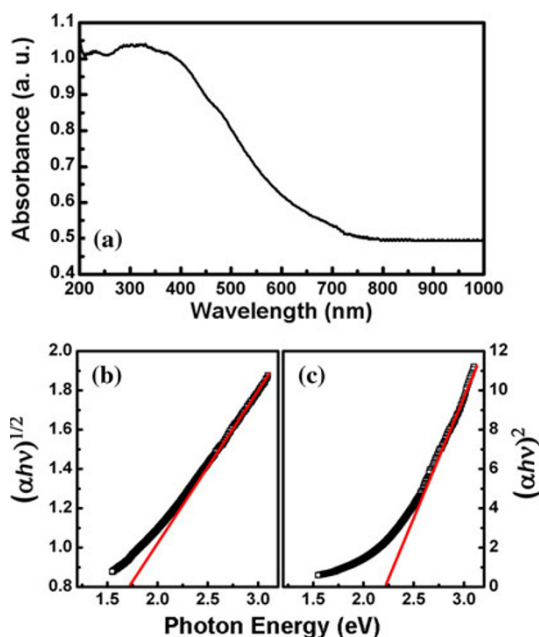


**Fig. 6** **a** The UV–vis absorption spectra **b** plots of  $(\alpha hv)^{1/2}$  and **(c)**  $(\alpha hv)^2$  vs  $h\nu$  for ZnFe<sub>2</sub>O<sub>4</sub> nanowire arrays

our result. At the same time, the image captured by camera indicates that the sample gives out blue-violet light, which is corresponding to the PL spectrum result. ZnFe<sub>2</sub>O<sub>4</sub> has been known to have the strong absorption in the UV–vis range [38–40]. As shown in Fig. 6, the ZnFe<sub>2</sub>O<sub>4</sub> nanowire arrays have the strong band edge absorption in the wavelength region of  $\leq 700$  nm. The optical band gap  $E_g$  can be estimated from absorption coefficient ( $\alpha$ ) using the Tauc relation

$$\alpha hv = A(hv - E_g)^q$$

where  $A$  is a constant that depends on the transition probability,  $h\nu$  is the energy of incident photon, and  $q$  is an

index that characterizes the optical absorption process [41]. It is well known that direct and indirect band gap energy for the semiconductor nanostructures can be obtained from the intersection of linear fits of  $(\alpha hv)^{1/q}$  versus  $h\nu$  plots for  $q = 1/2$  and 2 on the  $x$ -axis. Here, the estimated values of the direct and indirect band gaps are about 2.23 and 1.73 eV for preferred oriented ZnFe<sub>2</sub>O<sub>4</sub> nanowire arrays, respectively (shown in Fig. 6b and c). Improved optical properties of the ZnFe<sub>2</sub>O<sub>4</sub> nanomaterials are expected, and these aspects need further investigation.

## Conclusion

In summary, arrays of ZnFe<sub>2</sub>O<sub>4</sub> nanowires with diameters of about 16 nm were successfully fabricated by electro-deposition of Zn<sup>2+</sup> and Fe<sup>2+</sup> into AAO templates and post-oxidation annealing in atmosphere. The results of XRD and HRTEM exhibit that the nanowires have the bcc structure with [110] as the texture direction along the nanowire axis. The preferred orientation and shape anisotropy of the nanowire arrays makes the ZnFe<sub>2</sub>O<sub>4</sub> nanowire arrays to exhibit the uniaxial magnetic anisotropy with the easy magnetization direction along the nanowire axes. The optical properties show ZnFe<sub>2</sub>O<sub>4</sub> nanowire arrays give out blue-violet light, and the optical band gap  $E_g$  is estimated from absorption coefficient. Further investigation into magnetic and optical properties of the ZnFe<sub>2</sub>O<sub>4</sub> nanomaterials is in progress.

**Acknowledgments** This work is supported by National Science Fund for Distinguished Young Scholars (Grant No. 50925103), The Keygrant Project of Chinese Ministry of Education (Grant No. 309027) and The Fundamental Research Funds for the Central Universities (Grant No. Lzujbky-2009-162).

**Open Access** This article is distributed under the terms of the Creative Commons Attribution Noncommercial License which permits any noncommercial use, distribution, and reproduction in any medium, provided the original author(s) and source are credited.

## References

1. R.C.V. Gopal, S.V. Manorama, V.J. Rao, J. Mater. Sci. Lett. **19**, 775 (2000)
2. Z. Jiao, M.H. Wu, J.Z. Gu, Z. Qin, IEEE Sens. J. **3**, 435 (2003)
3. X.S. Niu, W.P. Du, W.M. Du, Sens. Actuators B **99**, 405 (2004)
4. X.F. Chu, X.Q. Liu, G.Y. Meng, Sens. Actuators B **65**, 64 (2000)
5. G.G. Liu, X.Z. Zhang, Y.J. Xu, X.S. Niu, L.Q. Zheng, X.J. Ding, Chemosphere **55**, 1287 (2004)
6. M. Sultan, R. Singh, J. Appl. Phys. **105**, 07A512 (2009)
7. F.F. Liu, X.Y. Li, Q.D. Zhao, Y. Hou, X. Quan, G.H. Chen, Acta Mater. **57**, 2684 (2009)
8. V. Sepelak, M. Zatroch, K. Tkacova, P. Petrovic, S. Wibmann, K.D. Becker, Mater. Sci. Eng. A. **22**, 226 (1997)

9. H. Ehrhardt, S.J. Campbell, M. Hofmann, *Scripta Mater.* **48**, 1141 (2003)
10. J. Philip, G. Gnanaprakash, G. Panneerselvam, M.P. Antony, T. Jayakumar, B. Raj, *J. Appl. Phys.* **102**, 054305 (2007)
11. M. Bohra, S. Prasad, N. Kumar, D.S. Misra, S.C. Sahoo, N. Venkataramani, R. Krishnan, *Appl. Phys. Lett.* **88**, 262506 (2006)
12. X.J. Xu, L.H. Zhou, Q.G. Zhai, C.Z. Lu, *J. Am. Ceram. Soc.* **90**, 1959 (2007)
13. S.A. Oliver, V.G. Harris, H.H. Hamdeh, J.C. Ho, *Appl. Phys. Lett.* **76**, 2761 (2000)
14. B. Jeyadevan, K. Tohji, K. Nakatsuka, *J. Appl. Phys.* **76**, 6325 (1994)
15. C. Upadhyay, H.C. Verma, V. Sathe, A.V. Pimpale, *J. Magn. Magn. Mater.* **312**, 271 (2007)
16. Y. Huang, X.F. Duan, Q.Q. Wei, C.M. Lieber, *Science* **29**, 630 (2001)
17. M.S. Gudiksen, L.J. Lauhon, J.F. Wang, D.C. Smith, C.M. Lieber, *Nature* **415**, 617 (2002)
18. A.J. Mieszawska, R. Jalilian, G.U. Sumanasekera, F.P. Zamborini, *Small* **3**, 722 (2007)
19. X.F. Han, S. Shamaila, R. Sharif, J.Y. Chen, H.R. Liu, D.P. Liu, *Adv. Mater.* **21**, 1 (2009)
20. L.E. Greene, M. Law, J. Goldberger, F. Kim, J.C. Johnson, Y.F. Zhang, R.J. Saykally, P.D. Yang, *Angew. Chem. Int. Ed.* **42**, 3031 (2003)
21. A. Ponrouch, S. Garbarino, S. Pronovost, P.L. Taberna, P. Simon, D. Guay, *J. Electrochem. Soc.* **157**, K59 (2010)
22. C. Eid, A. Brioude, V. Salles, J.C. Plenet, R. Asmar, Y. Monteil, R. Khoury, A. Khoury, P. Miele, *Nanotechnology* **21**, 125701 (2010)
23. Z.L. Wang, X.J. Liu, M.F. Lv, P. Chai, Y. Liu, X.F. Zhou, J. Meng, *J. Phys. Chem. C* **112**, 15171 (2008)
24. X.F. Chu, D.L. Jiang, C.M. Zheng, *Sens. Actuators B: Chem.* **123**, 793 (2007)
25. X.Y. Hou, J. Feng, X.D. Xu, M.L. Zhang, *J. Alloys. Compd.* **491**, 258 (2010)
26. S.X. Liu, K. Yue, K. Jiao, Y. Zhou, H.Y. He, *Mater. Lett.* **60**, 154 (2006)
27. G.Y. Zhang, C.S. Li, F.Y. Cheng, *Sens. Actuators B* **120**, 403 (2007)
28. Y.J. Kim, C.H. Lee, Y.J. Hong, G. Yi, S.S. Kim, H. Cheong, *Appl. Phys. Lett.* **89**, 163128 (2006)
29. B.D. Yao, Y.F. Chan, N. Wang, *Appl. Phys. Lett.* **81**, 22 (2002)
30. J. Zhang, G.A. Jones, T.H. Shen, S.E. Donnelly, G.H. Li, *J. Appl. Phys.* **101**, 054310 (2007)
31. Y.G. Zhu, X.C. Dou, X.H. Huang, L. Li, G.H. Li, *J. Phys. Chem. B* **110**, 26189 (2006)
32. Y. Xu, D.S. Xue, D.Q. Gao, J.L. Fu, X.L. Fan, D.W. Guo, B. Gao, W.B. Sui, *Electrochim. Acta* **54**, 5684 (2009)
33. D.Q. Gao, D.S. Xue, Y. Xu, Z.J. Yan, Z.H. Zhang, *Electrochim. Acta* **54**, 2392 (2009)
34. C.W. Yao, Q.S. Zeng, G.F. Goya, T. Torres, J.F. Liu, H.P. Wu, M.Y. Ge, Y.W. Zeng, Y.W. Wang, J.Z. Jiang, *J. Phys. Chem. C* **111**, 12274 (2007)
35. H.H. Hamed, J.C. Ho, S.A. Oliver, R.J. Willey, G. Olivieri, G. Busca, *J. Appl. Phys.* **81**, 1851 (1997)
36. A.K. Srivastava, M. Deepa, N. Bahadur, M.S. Goyat, *Mater. Chem. Phys.* **114**, 194 (2009)
37. A.J. Chen, X.M. Wu, Z.D. Sha, L.J. Zhuge, Y.D. Meng, *J. Phys. D Appl. Phys.* **39**, 4762 (2006)
38. Z.H. Yuan, W. You, J.H. Jia, L.D. Zhang, *Chin. Phys. Lett.* **15**, 535 (1998)
39. Z. Wu, M. Okuya, S. Kaneko, *Thin Solid Films* **385**, 109 (2001)
40. E. Marquez, J.R. Malo, P. Villares, R.J. Garay, P.J.S. Ewen, A.E. Owen, *J. Phys. D Appl. Phys.* **25**, 535 (1992)
41. A.F. Qasrawi, *Cryst. Res. Technol.* **40**, 610 (2005)